Petroleum Science 22 (2025) 5176–5188

Contents lists available at ScienceDirect

Petroleum Science

journal homepage: www.keaipublishing.com/en/journals/petroleum-science

Original Paper

Enhanced oil recovery with a thermo-thickening viscoelastic surfactant: A comparison with polymer

Mo-Yi Li [a], Quan Yin [a], Bo Li [b], Rui-Bo Cao [b], Yan Zhang [a], Xue-Zhi Zhao [a,*], Yu-Jun Feng [a,**]

[a] Polymer Research Institute, State Key Laboratory of Advanced Polymer Materials, Sichuan University, Chengdu, 610065, Sichuan, People's Republic of China

[b] EOR Laboratory, Exploration & Development Research Institute of Daqing Oilfield Company of PetroChina, Daqing, 163712, Heilongjiang, People's Republic of China

ARTICLE INFO

Article history:
Received 4 February 2025
Received in revised form
27 July 2025
Accepted 4 August 2025
Available online 8 August 2025

Edited by Yan-Hua Sun

Keywords:
Viscoelastic surfactant
Thermo-thickening
Enhanced oil recovery
Polymer flooding

ABSTRACT

High-molecular-weight partially hydrolyzed polyacrylamide (HPAM) has extensively used in enhanced oil recovery (EOR) process; however, it suffers from poor injectivity into low-permeability oil reservoirs and compromised long-term thermal stability under reservoir conditions. To address these challenges, a viscoelastic surfactant, 3-(*N*-erucamidopropyl-*N*,*N*-dimethyl ammonium) betaine (EDAB), was developed and systematically compared with HPAM. Experimental results demonstrate that EDAB outperforms HPAM in thermal resilience, salt tolerance, and interfacial activity. Unlike HPAM's thermal thinning behavior, EDAB displays thermo-thickening properties, with viscosity rising from 225 to 366 mPa·s as temperature increases from 25 to 55 °C. EDAB maintains 100% viscosity retention under 80 mg·L^{-1} Ca^{2+} or Mg^{2+}, whereas HPAM experiences 46% viscosity loss under identical ionic conditions. Core-flooding tests conducted under simulated Daqing oil reservoir conditions indicate that EDAB achieves a 1.4% higher incremental oil recovery factor than HPAM with equal initial solution concentration. When HPAM was employed as a mobility control for pre- or post-flush, EDAB elevates the recovery factor by 13.9% over water flooding. These comparative analyses underscore the potential of EDAB as a thermally stable, salt-insensitive alternative to HPAM, offering an optimized chemical strategy for EOR in challenging reservoir environments. The findings provide empirical validation for surfactant-based solutions to address HPAM's operational constraints in low-permeability formations.
© 2025 The Authors. Publishing services by Elsevier B.V. on behalf of KeAi Communications Co. Ltd. This is an open access article under the CC BY license (http://creativecommons.org/licenses/by/4.0/).

1. Introduction

Approximately two thirds of the original oil in place still remain in reservoirs after conventional primary (self-flow by natural forces) and secondary (re-pressurization using water flooding in most cases) production (Lake et al., 1992; Sandrea and Sandrea, 2007; Jafarbeigi et al., 2022). Much of the residual oil could be further produced by the enhanced oil recovery (EOR) process (Thomas, 2008; Al-Asadi et al., 2023; Zamani et al., 2024), among which chemical flooding represents one of the most effective procedures, and has been most frequently employed in China (Chang et al., 2006).

Chemical flooding involves injecting displacing fluids into reservoirs through injection wells to mobilize crude oil toward production wells. The process primarily utilizes surfactants and water-soluble polymers in formulated solutions. Simultaneous injection of these components creates synergistic effects: surfactants reduce interfacial tension (IFT), while polymers enhance solution viscosity for improved mobility control (Jain et al., 2022; Han et al., 2022). This combined action enables oil displacement through dual mechanisms—capillary force reduction and viscous force amplification (Raffa et al., 2016; Ahmed et al., 2023). Termed surfactant-polymer (SP) binary flooding, this technique has demonstrated technical viability as an enhanced oil recovery method. Its efficacy has been systematically validated through numerical simulations (Rai et al., 2009), laboratory experiments, and field applications in multiple Chinese oilfields (Sun et al., 2020).

* Corresponding author.
** Corresponding author.
E-mail addresses: zhaoxz@scu.edu.cn (X.-Z. Zhao), yjfeng@scu.edu.cn (Y.-J. Feng).

Peer review under the responsibility of China University of Petroleum (Beijing).

https://doi.org/10.1016/j.petsci.2025.08.007
1995-8226/© 2025 The Authors. Publishing services by Elsevier B.V. on behalf of KeAi Communications Co. Ltd. This is an open access article under the CC BY license (http://creativecommons.org/licenses/by/4.0/).

However, from a chemical perspective, certain adverse interactions impede the success of SP modes in reservoirs with divalent cations. The predominant EOR polymer, high-molecular-weight partially hydrolyzed polyacrylamide (HPAM) (Chen et al., 2023; Seright and Wang, 2023), exhibits inherent limitations: susceptibility to viscoelastic degradation in brines containing Ca^{2+} and Mg^{2+} (Akstinat, 1980; Zaitoun and Poitie, 1983) and thermal instability under reservoir temperatures (Muller, 1981a, 1981b). Additionally, HPAM demonstrates pronounced mechanical vulnerability to irreversible shear-induced chain scission during flow through porous media (Seright, 1983; Chauveteau and Sorbie, 1991; Li et al., 2020), causing molecular weight reduction, polydispersity expansion, and consequent permanent viscosity loss.

Petroleum sulfonates and synthetic alkylaryl-sulfonates are preferred surfactants in SP formulations due to their cost-effectiveness and significant IFT reduction capabilities. However, their limited electrolyte stability, particularly against divalent cations in reservoir brines, presents operational constraints. Early studies (Bansal and Shah et al., 1978a, 1978b; Kumar et al., 1984) documented a concentration-dependent IFT elevation in petroleum sulfonate solutions when exposed to $CaCl_2$ or $MgCl_2$ in connate water. Agharazi-Dormani et al. (1990) further identified viscous precipitates formed through cation-surfactant interactions at ambient conditions. Such loss of IFT not only compromises interfacial activity essential for oil mobilization, but also exacerbates recovery challenges through viscosity degradation effects.

To obviate the above limitations of polymers and surfactants presently used, Lakatos et al. (2007) reported laboratory results of viscoelastic surfactant (VES) gel as mobility controlling agent in tertiary oil recovery. Such a gel is mainly composed of an alkyl-aryl sulfonate and the commodity nonionic surfactant ORS-64, achieving IFT reduction to 10^{-1} mN·m^{-1} magnitude. The gel demonstrated significantly enhanced resistance to thermal and shear degradation compared to conventional synthetic and natural polymer-based systems. Core flooding experiments demonstrated approximately 10% incremental oil recovery through simultaneous IFT reduction and mobility regulation, with potential improvements in microscopic displacement efficiency. Morvan et al. (2009) developed a viscoelastic surfactant (VES) fluid displaying viscosity-phase transitions at elevated temperatures and low surfactant concentrations in high-salinity brines (39,000 mg·L^{-1} TDS seawater or 20,000 mg·L^{-1} NaCl). The system exhibited brine-insensitive viscosity (3–15 mPa·s), 50 μg·g^{-1} surfactant adsorption in Clashach sandstone at 80 °C, and 29% incremental oil recovery over water flooding. However, the limited salt tolerance of these VESs, particularly toward multivalent cations, restricts its applicability to reservoirs in high total dissolved solids (TDS).

Xu et al. (2021) developed a novel Gemini VES (VES-Q) with erucyl amide tails and a cyclodextrin spacer. The bulky cyclodextrin group introduces steric hindrance, lowering the surfactant packing parameter (*P*) and reducing ion-induced dehydration. While VES-Q demonstrates stable viscosity (> 50 mPa·s) in high-salinity brines (Ca^{2+} or Mg^{2+} > 8000 mg·L^{-1})—outperforming conventional cationic VES systems—its practical use in high-temperature reservoirs remains limited due to its required high concentration and moderate thermal tolerance.

In contrast, Huang et al. (2022) designed a polyhydroxy cationic VES (SY-TO) with multiple hydroxyl groups in its hydrophilic head. This design strengthens the hydration layer, counteracting ion dehydration and maintaining stable wormlike micelles (WLMs) in extreme brines (> 14 wt% KCl or 10 wt% $CaCl_2$). Notably, SY-TO retains high viscosity (> 50 mPa·s) even at 140 °C, a property attributed to its dynamic aggregation-dissociation equilibrium under thermal molecular motion. These features position SY-TO as a promising candidate for fracturing in harsh reservoir conditions.

Microscopically, VES gels derive from entangled WLMs, flexible cylindrical aggregates formed by surfactant self-assembly above critical concentrations (Dreiss, 2007; Chu and Feng, 2011). These transient networks mimic polymer solutions, enabling broad applications (Yang, 2002). While conventional WLMs developed from cationic surfactants with hydrophobic tail less than C_{16} (Dreiss, 2007), recent advances focus on C_{22}-tailed cationic (Raghavan and Kaler, 2001; Croce et al., 2005) and zwitterionic (Kumar et al., 2007; Chu et al., 2010a, 2010b) surfactants, typically requiring salt or hydrotropic additives. Our prior work synthesized C_{22}-tailed anionic WLMs (Han et al., 2011) and ultra-long-chain amidosulfobetaines (Chu and Feng, 2009), revealing salt-free zwitterionic WLM formation and stimuli-responsive rheology (Chu et al., 2010; Chu and Feng, 2010a, 2010b, 2011). However, comparative advantages of VES over conventional HPAM polymers remain unverified, necessitating systematic evaluations under reservoir conditions. Very recently, we found a C_{22}-tailed betaine surfactant, 3-(*N*-erucamidopropyl-*N*,*N*-dimethyl ammonium) betaine (EDAB) exhibits a unique, abnormal thermo-thickening ability at 25–55 °C (Yin et al., 2022), which exactly falls in the typical oil reservoir temperature of Daqing Oilfield.

This study systematically compared EDAB with a conventional HPAM (M_η = 1.2 × 10^7 g·mol^{-1}) regarding thickening ability, rheological behavior, IFT, long-term thermal stability, injectivity in porous media, as well as their ability to increase oil recovery factor, under simulated Daqing Oilfield conditions. The comparative analysis provides essential data to assess EDAB's potential as a viable alternative for practical use, particularly for low-permeability reservoirs where conventional HPAM exhibits constrained efficacy.

2. Experimental section

2.1. Materials

The surfactant used, 3-(*N*-erucamidopropyl-*N*,*N*-dimethyl ammonium) betaine (EDAB, Scheme 1; molecular formula: $C_{29}H_{56}N_2O_3$; molecular weight: 480.43; purity: 99%), was synthesized in previous work (Yin et al., 2022). HPAM (Scheme 1) kindly offered from Beijing Hengju Group has molecular weight 1.2 × 10^7 g·mol^{-1} and hydrolysis degree of 29%.

The reagents NaCl, $CaCl_2$, and $MgCl_2$, of analytical purity, were obtained from Chron Chemicals (Chengdu, China). The laboratory water used was ultrapure water with a resistivity of 18.25 MΩ·cm. The natural rock core was supplied by the Exploration and Development Research Institute of Daqing Oilfield, China National Petroleum Corporation. The crude oil, with a viscosity of 9.8 mPa·s

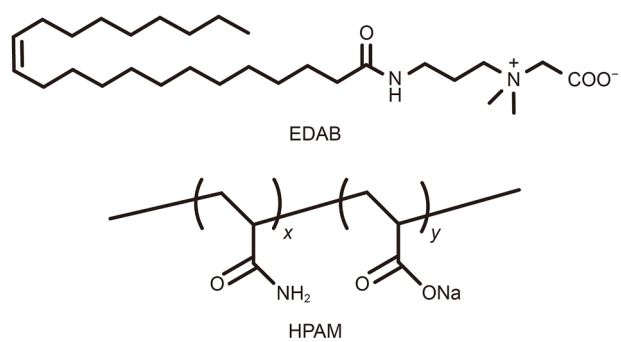

Scheme 1. Chemical structures of surfactant EDAB and polymer HPAM used in this work.

at 45 °C after dehydration and degassing, was supplied by Daqing Oilfield.

2.2. Preparation of solutions

The solvent used is 4500 mg·L^{-1} NaCl synthetic brine to simulate the salinity of typical Daqing oil reservoir. A measured amount of EDAB or HPAM powder was added to the vortex of brine under agitation for 30 min. The resulting dispersions were then shaken for 24–36 h (100 rpm, 25 °C) to achieve homogeneous solutions, which were left overnight before measurement.

For the salinity resistance evaluation, the surfactant or polymer concentration remains fixed at 2000 mg·L^{-1}, while the salinity varies according to the experimental design. The dissolution procedure follows the same protocol as described earlier.

2.3. Rheological test

Rheological experiments were carried out on a Physica MCR 301 (Anton Paar, Austria) rotational rheometer at 45±0.1 °C, and a solvent trap was used to minimize water evaporation. A Searle-type concentric cylinder geometry CC27 (ISO3219) with measuring bob radius of 13.33 mm and measuring cup radius of 14.46 mm was applied for all the test.

The first normal stress differences (N_1) of solutions were measured using a Physica MCR 302 rheometer with a cone-and-plate geometry (50 mm diameter, 1° cone angle). Shear rate was incrementally increased from 1 up to 3000 s^{-1}.

To investigate the shear resistance of EDAB and HPAM, the specimens were sheared at 12,000 rpm for 60 s at room temperature using a mixing speed governor (WT-VSA2000B, China). Then, the apparent viscosity of the sheared solutions was measured at 45 °C after different resting times.

2.4. IFT measurement

The IFT between the sample solution and oil phase was measured using a TX500C interfacial tensiometer (CNG, USA). Prior to analysis, the measurement tube was sequentially cleaned with isopropanol and preconditioned through multiple rinses with the test solution. The tube was then filled with the sample solution, followed by precise injection of crude oil into its axial center using a microliter syringe. The tube was sealed and positioned in the instrument's measurement chamber, with care taken to prevent air bubble formation or oil adhesion to the tube walls. IFT values were calculated via digital droplet analysis, utilizing recorded dimensions (length and width) of the suspended oil droplet. Experimental parameters included: temperature maintained at 45 °C, rotational speed fixed at 5,000 rpm, and imaging intervals programmed at 1-min increments for the initial 30 min, transitioning to 3-min intervals thereafter.

2.5. Long-term thermal aging

Identical concentrations (2000 mg·L^{-1}) of EDAB and HPAM solutions were prepared in synthetic brine (4400 mg·L^{-1} NaCl, 50 mg·L^{-1} $CaCl_2$, 50 mg·L^{-1} $MgCl_2$, total salinity 4500 mg·L^{-1}) for long-term thermal stability monitoring. N_2 was bubbled into the solutions for 1 h to displace oxygen inside. The surfactant or polymer solution is distributed into a series of sample vials and stored in an oven at 45 °C. At regular intervals over a 60-d period, one vial from each group is removed and viscosity is monitored using the MCR rheometer described above.

2.6. Core flooding test

To evaluate the performance of EDAB and HPAM solutions, crude oil recovery experiments were conducted using the experimental setup described in Fig. 1. The experimental setup consisted of a nitrogen bottle, a syringe pump, a cylinder holding the displacing fluid, a core holder, and an effluent collector.

2.6.1. Basic parameters of the cores

Before conducting core flooding tests, the basic parameters of the core were determined. The length (L) and diameter (d) of the cores were measured, followed by vacuum drying at 45 °C to a constant weight m_0. The core was saturated with synthetic brine (4500 mg·L^{-1} NaCl) using ZB-IV vacuum pressurized saturation device (ETUSE, Changzhou, China). The core was first vacuumed in the vacuum pressurized saturation device for 12 h, followed by

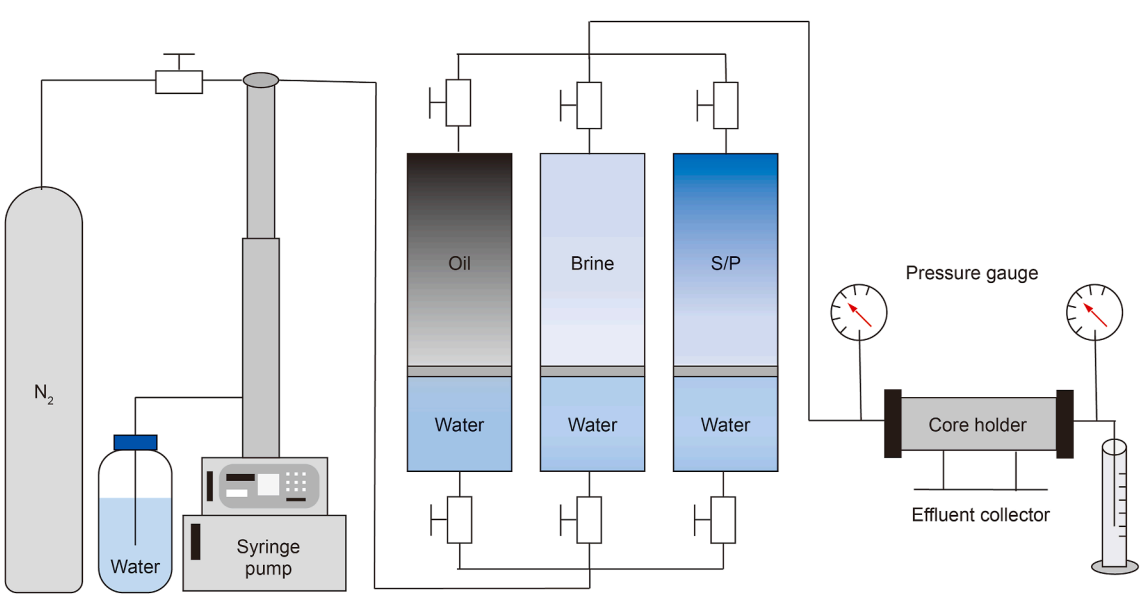

Fig. 1. Schematic diagram of core flooding test apparatus.

brine injection to initiate saturation. The saturation process lasted 12 h, with the pressure maintained at 10 MPa. The weight of the core was measured after saturation was completed and recorded as m_1, and then the pore volume (PV) and porosity (ϕ) of the core were calculated using the following equations:

$$\mathrm{PV} = \frac{m_1 - m_0}{\rho_\mathrm{w}} \tag{1}$$

$$\phi = \frac{\mathrm{PV}}{\pi d^2 L / 4} \times 100\% \tag{2}$$

where ρ_w is the density of the brine, g·cm^{-3}.

2.6.2. Injectivity test

The brine-saturated core was placed into a core holder, with the confining pressure maintained at 4 MPa. The core was injected with synthetic brine (4500 mg·L^{-1} NaCl) for a certain period of time to keep the core saturated while the temperature was increased to 45 °C until the inlet pressure was stabilized. Brine was injected at a rate of 0.2 mL·min^{-1}, the stabilized water flooding pressure was recorded, and permeability was calculated using Darcy's equation:

$$Q = K \frac{A \Delta P}{\eta L} \tag{3}$$

where η is the fluid viscosity, mPa·s; K is the permeability of the pore medium, D; ΔP is the pressure drop across the core, 10^{-1} MPa; A is the cross-sectional area flow area, cm^2; and Q is the volumetric flow rate under the applied pressure gradient, cm^3·s^{-1}.

The polymer or surfactant solution was injected into the core at a rate of 0.2 mL·min^{-1} until the pressure was stabilized. The final differential pressure was recorded and the resistance factor (RF) was calculated (Eq. (4)).

$$\mathrm{RF} = \frac{K_\mathrm{w}/\eta_\mathrm{w}}{K_\mathrm{p(s)}/\eta_\mathrm{p(s)}} = \frac{Q_\mathrm{w}}{Q_\mathrm{p}} \times \frac{\Delta P_\mathrm{p(s)}}{\Delta P_\mathrm{w}} \tag{4}$$

where $\Delta P_\mathrm{p(s)}$ and ΔP_w are the differential pressures during polymer flooding (or surfactant flooding) and water flooding, respectively, MPa; $\eta_\mathrm{p(s)}$ and η_w correspond to the viscosity of the polymer solution (or surfactant solution) and brine, mPa·s; while $K_\mathrm{p(s)}$ and K_w correspond to the permeability of the polymer solution (or surfactant solution) and brine during core flow, mD.

Subsequently, brine was injected into the core at a rate of 0.2 mL·min^{-1} until the displacement pressure was stabilized. The pressure difference before and after the final core was recorded, and the residual resistance factor (RRF) was calculated via Eq. (5):

$$\mathrm{RRF} = \frac{K_\mathrm{wb}}{K_\mathrm{wa}} \tag{5}$$

where K_wb and K_wa are the aqueous-phase permeability before and after injection of the polymer (or surfactant) solution, respectively, mD.

2.6.3. Polymer and surfactant flooding tests

The cores saturated with synthetic brine (4500 mg·L^{-1} NaCl) were placed in a core holder, with the confining pressure maintained at 4 MPa and the temperature set to 45 °C for 1 h. Crude oil was injected at a rate of 0.2 mL·min^{-1} until the effluent oil cut reached 100% within a certain period of time, at which point the total water volume (V_0) in the effluent collector was recorded, representing initial oil saturation. Subsequently, simulated brine was injected at a rate of 0.2 mL·min^{-1} until the water cut in the effluent was more than 98%. At this point, the volume of oil in the effluent collector (V_w) was recorded, and the water flooding recovery factor (E_w) was calculated from Eq. (6). Then, 0.5 PV of displacing fluid (either polymer or surfactant solution) was injected at a rate of 0.2 mL·min^{-1}. Finally, synthetic brine (4500 mg·L^{-1} NaCl) was injected at a rate of 0.2 mL·min^{-1} to start the post water flooding until the water cut in the effluent exceeded 98%. At this time record the volume ($V_\mathrm{p(s)}$) of oil produced from the effluent collector. Eq. (6) is also used to calculate the polymer flooding recovery factor (E_p) or surfactant flooding recovery (E_s).

$$E_i = \frac{V_i}{V_0} \times 100\% \tag{6}$$

where E_i represents the water recovery factor (E_w), polymer flooding recovery factor (E_p) or surfactant flooding recovery (E_s); V_i indicates the volume of oil produced in water flooding (V_w), and the volume of oil produced in chemical flooding ($V_\mathrm{p(s)}$), mL; and V_o is the total volume of crude oil in the core, mL.

3. Results and discussion

3.1. Thickening ability of EDAB and HPAM

Thickening ability is crucial for a polymer or VES to be used in displacing oil, as the viscosity of the displacing fluid plays a key role in regulating the mobility ratio between displacing fluid and displaced oil, thus determining the sweep efficiency, finally the oil recovery factor (Manichand and Seright, 2014). Therefore, the thickening ability of EDAB and HPAM is compared under Daqing oil reservoir condition, concerning the chemical concentration, salinity and temperature.

3.1.1. Effect of chemical concentration

As exhibited in Fig. 2, the apparent viscosity (η) of both HPAM and EDAB solutions increases with their concentrations (C). When the concentration is below 2000 mg·L^{-1}, the viscosity of HPAM solution is slightly lower than that of EDAB solution. However, as

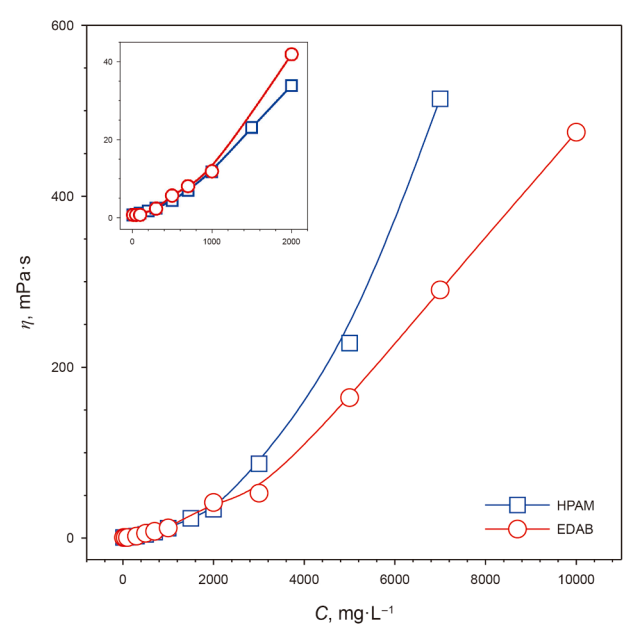

Fig. 2. Comparison of thickening ability of EDAB and HPAM for 4,500 mg·L^{-1} NaCl solution at 45 °C and shear rate of 10 s^{-1}.

the concentration exceeds 2000 mg·L^{-1}, the thickening ability of HPAM significantly surpasses that of EDAB. This difference can be attributed to the formation of a WLMs network by EDAB at lower concentrations (Yin et al., 2022), which closely resembles the entangled network of HPAM molecular chains. At higher concentrations, HPAM can entangle to form a denser network. While EDAB also forms longer WLMs at high concentrations, the dynamic equilibrium of "breakage-reformation" within these micelles leads to lower viscosity than HPAM. The thickening ability of HPAM and EDAB can be delineated at 2000 mg·L^{-1}. Considering the requirements of practical use for low concentration and high viscosity, we ultimately selected 2000 mg·L^{-1} of both HPAM and EDAB for subsequent experiments. At this concentration, the apparent viscosity of the HPAM and EDAB solutions is 37 and 41 mPa·s, respectively.

3.1.2. Effect of salinity and divalent cations

Generally, the connate formation water of oil reservoirs contains Na^+ and multivalent cations like Ca^{2+} and Mg^{2+}, which shield electrostatic repulsion among the carboxylate groups along HPAM skeleton, causing collapse and aggregation of polymer chains, reducing hydrodynamic volume of polymer coil and lowering viscosity of polymer solution (Iyer et al., 2021). For instance, HPAM with a molecular weight of 15 million Dalton loses mor than 80% of its apparent viscosity in 10,000 mg·L^{-1} NaCl, undermining its efficiency to improve mobility ratio thus impairing its ability to enhance oil recovery (Li, 2015). Therefore, it is an indispensable to examine the impact of salinity and polyvalent cations on viscosity buildup of any chemicals used for EOR process.

First, the effect of Na^+ on the thickening ability of HPAM and EDAB was investigated. As shown in Fig. 3(a), with elevation of NaCl concentration from 0 to 4500 mg·L^{-1}, the apparent viscosity of the HPAM solution at 2000 mg·L^{-1} decreases sharply, from 326.0 to 33.8 mPa·s, with 89.6% of loss in viscosity. This is attributed to the weakening of electrostatic interactions between HPAM molecular chains as the NaCl concentration increases. When further increasing NaCl concentration to 15,000 mg·L^{-1}, the decrease in viscosity slowed down significantly from 33.8 to 19.3 mPa·s, which was only 4.4%. This indicates that the electrostatic shielding effect of NaCl on the HPAM molecular chains gradually approaches saturation, causing the viscosity to stabilize.

On the contrary, within the whole salinity investigated (from 0 to 15,000 mg·L^{-1} NaCl), the apparent viscosity of EDAB solution remains unchanged, always at 41 mPa·s irrespective of the salinity. As a betaine surfactant, the stoichiometric cationic and anionic groups in EDAB attract electrostatically; when NaCl is introduced, such an attraction is shielded by both Na^+ and Cl^-, making the headgroups aggregate together; in other words, the EDAB molecules are readily assembling into wormlike micelles, showing strong thickening ability macroscopically.

Furthermore, the effect of divalent cations on the apparent viscosity of HPAM and EDAB solutions was examined. As exhibited in Fig. 3(b), the apparent viscosity of the EDAB solution remains almost unchanged whatever the alteration of Ca^{2+} and Mg^{2+}, stabilizing at around 41 mPa·s. This indicates that divalent cations do not affect the thickening ability of EDAB solution, as these cations cannot be complexed with carboxylate groups in EDAB molecule, owing to the stoichiometric attraction between positive ammonium and negative carboxylate.

In contrast, low concentrations (0–10 mg·L^{-1}) of Ca^{2+} and Mg^{2+} initially increase the viscosity of the HPAM solution, while further increases in their concentration leads to a significant decrease in viscosity. When the concentration of Ca^{2+} and Mg^{2+} reaches 80 mg·L^{-1}, the viscosity of the HPAM solution drops to 21.6 mPa·s, with a viscosity retention (R_η, percentage of changed viscosity relative to initial viscosity) of 63.5%. The reduction in viscosity at high concentration of Ca^{2+} and Mg^{2+} is related to electrostatic shielding, whereas the increase in viscosity at low dosage may be attributed to weak complexation among these divalent cations and carboxylate groups along HPAM main chains (Pu et al., 2016). As the divalent cations Ca^{2+} and Mg^{2+} can simultaneously create electrostatic attractions with two carboxylate groups on the HPAM molecular chains, resulting in weak cross-linking between the chains and thereby enhancing the viscosity of the solution.

3.1.3. Effect of temperature

The change in temperature from surface to bottomhole, from borehole to reservoir, will also significantly affects the performance of chemicals used in EOR process (Belhaj et al., 2020). Therefore, we further investigated the impact of temperature on the apparent viscosity of HPAM and EDAB solutions.

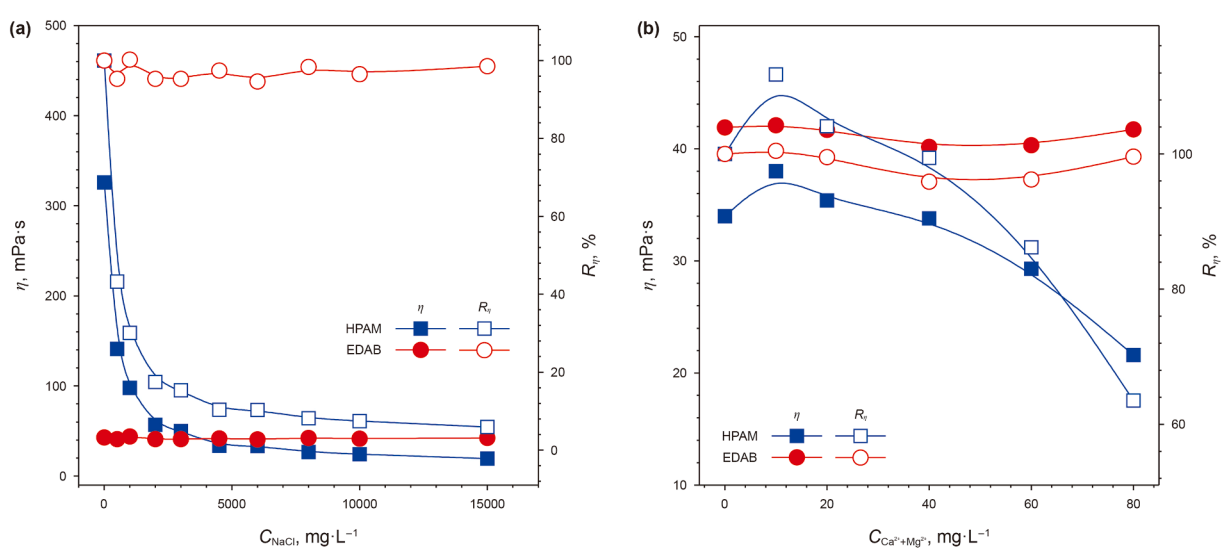

Fig. 3. The effect of salinity on apparent viscosity of 2000 mg·L^{-1} HPAM and EDAB solutions measured at 45 °C and a shear rate of 10 s^{-1}. (**a**) NaCl; (**b**) divalent cations (Ca^{2+} and Mg^{2+} in a 1:1 mass ratio) added to 4500 mg·L^{-1} NaCl solution.

Fig. 4 shows the apparent viscosity profile of 2000 mg·L^{-1} EDAB and HPAM solutions in the temperature range of 20–80 °C. One can find that the viscosity of the HPAM solution decreases gradually with increasing temperature, exhibiting typical "thermo-thinning" phenomenon, as always evidenced in the literature results (Yang, 2001). When the temperature rises from 25 to 45 °C, the viscosity decreases from 41 to 33 mPa·s, resulting in a viscosity retention rate of 80.5%. Further increasing the temperature to 80 °C results in a final viscosity of 22 mPa·s, with a viscosity retention rate of only 53.7%.

In contrast, the viscosity of the EDAB solution initially increases with rising temperature before subsequently decreasing, demonstrating a "thermally thickening" behavior. At 25 °C, the viscosity of the EDAB solution is 28 mPa·s, then increases to 37 mPa·s at 45 °C, marking 32.1% of enhancement. Upon further heating to 55 °C, the viscosity peaks at 53 mPa·s, with an increase of 89.3%. However, at 80 °C, the viscosity drops to 15 mPa·s, with a viscosity retention rate of 53.5%, which is very close to that of HPAM. The thermo-thinning of the HPAM solution is attributed to the dehydration-induced coiling of the polymer chains at high temperatures (Gao, 2013), while the thermally thickening behavior of EDAB is due to the increased persistence length (l_p) of the WLMs within the solution (Yin et al., 2022). The sharp viscosity decrease in EDAB solutions above 55 °C occurs because the persistence length of its wormlike micelles—after initially increasing with temperature—declines rapidly beyond this point (Yin et al., 2022). This persistence length reduction diminishes micellar rigidity and hydrodynamic volume, lowering viscosity. Similar behavior has been reported in studies of wormlike micelles by Zhang et al. (2015) and Raghavan and Kaler (2001). Therefore, from the viscosity–temperature curve, EDAB shows superior thermal stability at around 45 °C (Daqing oil reservoir temperature), highlighting its potential for application under this reservoir condition.

3.2. Rheological behavior of EDAB and HPAM solutions

During practical applications such as dissolution, dispersion, and pumping, the polymer molecules in displacing fluid are subjected to varying degrees of shear. In low to medium permeability oil reservoirs, these solutions also experience significant shear and elongation when flowing through porous media (Lai et al., 2016). Therefore, we compared the rheological behavior of HPAM and EDAB solutions.

3.2.1. Shear-thinning behavior

Fig. 5 indicates the flow curves of 2000 mg·L^{-1} EDAB and HPAM solutions. One can immediately find that both curves can be divided into three parts: Newtonian plateau at low shear rate region, shear-thinning slope at intermediate shear rate regime, and a second Newtonian plateau at high shear rate. More importantly, both curves can be fitted perfectly with the classical Carreau model (in set of Fig. 5). However, there are also some differences between two solutions. First, the first critical shear rate ($\dot{\gamma}_1^*$) of EDAB solution (0.003 s^{-1}) at which Newtonian plateau transits to shear thinning appears one order of magnitude earlier than that of HPAM solution (0.025 s^{-1}). This is understandable, as the physical supramolecular aggregates self-assembled from small surfactant molecules are more readily ruptured than the entanglements of long HPAM chains. The second difference comes from the shear-thinning degree of the solution; that is, the degree of viscosity reduction over a range of shear rate intervals, which can be quantitatively characterized by the power-law index, n, of the Carreau equation. EDAB solutions exhibit pronounced shear-thinning behavior, meaning their viscosity decreases more significantly under shear compared to their resting state. This property offers practical advantages: easier pumping and injection from the surface to the wellbore with reduced power requirements, and improved flow through reservoir pore throats, where shear-induced disassembly of worm-like assemblies prevents blockages and enhances deeper penetration. The third difference comes from the second critical shear rate ($\dot{\gamma}_2^*$), which is the junction between the shear-thinning region and the second Newtonian plateau region, above which the viscosity of both solutions decreases to about 6 mPa·s and remains constant; in other words, even if the assemblies are disassembled, the 2000 mg·L^{-1} EDAB solution still has the ability to regulate the flow. It is noteworthy, however, that $\dot{\gamma}_2^*$ of EDAB (215 s^{-1}) still appeared a bit

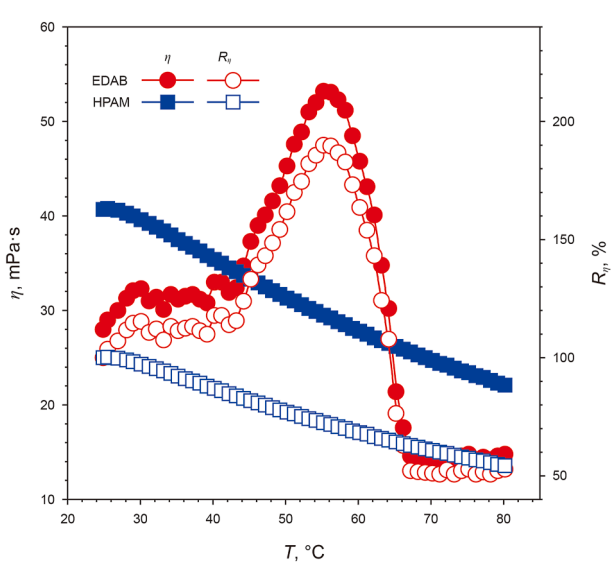

Fig. 4. Apparent viscosity of 2000 mg·L^{-1} EDAB and HPAM solutions plotted as a function of temperature. TDS, 4500 mg·L^{-1} NaCl; $\dot{\gamma}$, 10 s^{-1}.

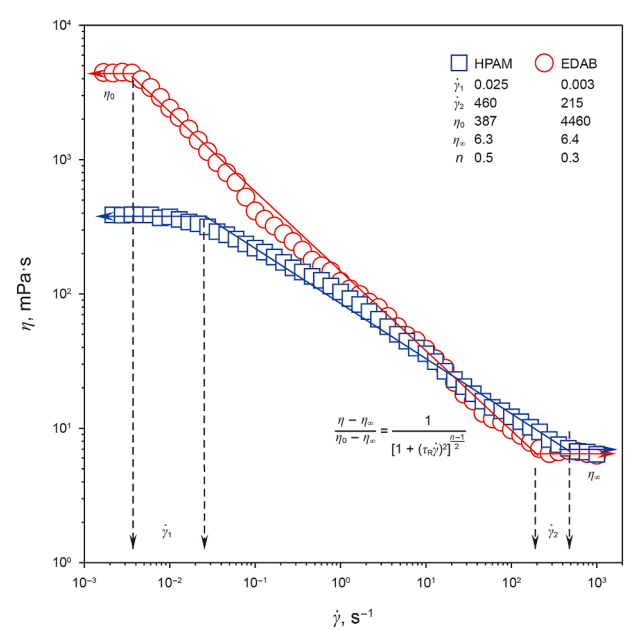

Fig. 5. Steady viscosity of 2000 mg·L^{-1} EDAB and HPAM solution as a function of shear rate. TDS, 4500 mg·L^{-1} NaCl; T, 45 °C. Solid lines represent Carreau model fits, where η_0 and η_∞ are the viscosity at zero and infinite shear plateaus, respectively.

earlier than that of HPAM (460 s^{-1}), but the gap narrowed to a factor of two.

We further compared the shear resistance of EDAB and HPAM solutions through shear degradation tests. As shown in Fig. S1, after 60 s of shearing at 12,000 rpm, the viscosity (41 mPa·s) of the 2000 mg·L^{-1} EDAB solution remained almost unchanged, with 100% viscosity retention rate. However, for the same concentration of HPAM solution, the viscosity decreased from the initial value (36 mPa·s) to 20.5 mPa·s after high-speed shear and its viscosity retention rate was only 56.9%. This observation suggests that the surfactant EDAB has better resistance to shear degradation than the polymer HPAM.

3.2.2. The first normal force

As current research demonstrates, the elastic properties of displacing fluids play a significant role in enhanced oil recovery (Wang et al., 2000). Zhong et al. (2022) established that these elastic effects substantially influence the viscosity of displaced phases. Furthermore, viscoelasticity has been shown to improve microscopic displacement efficiency (Ameli et al., 2019), with viscoelastic fluids finding widespread application in oilfield development (Masuda et al., 1992; Zeynalli et al., 2023; Xue et al., 2024). These findings underscore the importance of investigating the viscoelastic properties of both EDAB and HPAM solutions. However, the tiny elasticity of dilute solution cannot be determined from elastic modulus (Fig. S2). Therefore, the first normal stress difference (N_1), the difference between the principal stress and the stress at its vertical direction (as illustrated in Fig. S3), was selected here to quantitatively describe the viscoelasticity of EDAB and HPAM solutions within a shear rate range of 1–3000 s^{-1}.

As displayed in Fig. 6, with increasing shear rate, N_1 of both EDAB and HPAM solutions initially remains constant when the shear rate is less than 10 and 40 s^{-1}, indicating that the micellar structure in the EDAB solution is disrupted under lower stress, leading to a loss in viscosity. It is noteworthy that the N_1 of the EDAB solution begins to rise at a shear rate of 10 s^{-1}, which aligns with the shear rates typically encountered in actual oil

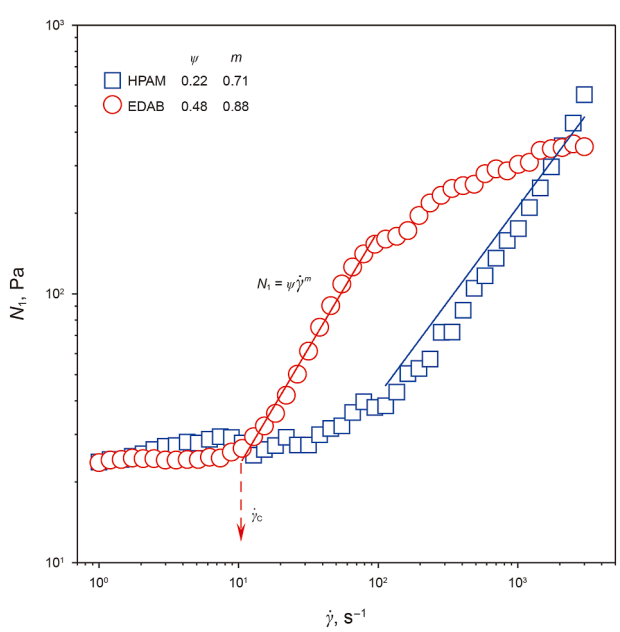

Fig. 6. The first normal stress differences (N_1) of 2000 mg·L^{-1} HPAM and EDAB solutions with TDS of 4500 mg·L^{-1} NaCl at 45 °C. The constants ψ and m are obtained by fitting the experimental data.

displacement processes. Furthermore, the N_1 of the EDAB solution is greater than that of the HPAM solution, suggesting that during the actual displacement process, the EDAB solution exhibits better viscoelasticity. The characteristic correlation constant ψ of the material and the exponent of the effect of shear rate on stress m can be obtained from the fitting of the experimental data. EDAB has a higher value of ψ (0.48) and a larger value of m (0.88), which indicates that EDAB exhibits a stronger stress enhancement effect during the flow process. Whereas, HPAM has a lower value of ψ (0.22) and a smaller value of m (0.71), indicating that it is less viscoelastic.

Additionally, when the shear rate exceeds the critical value, N_1 for both the EDAB and HPAM solutions begins to increase. At this point, the relaxation time (τ_R) of the solution can be described by the following equation (Zilz et al., 2014):

$$\tau_R = \frac{\psi}{2\eta_0} \tag{7}$$

where ψ is a constant; and η_0 represents the zero-shear viscosity of the solution. Based on Eq. (7), the relaxation time of 2000 mg·L^{-1} EDAB and HPAM solutions calculated is 0.54 and 0.28 s, respectively. The longer relaxation time for EDAB solution indicates that it possesses stronger elasticity compared to the HPAM solution.

3.3. Dynamic IFT

Reduction in IFT between oil and water phases is one of the key mechanisms for surfactant EOR (Ahmed et al., 2023). Therefore, the ability of EDAB to lower IFT was investigated in comparison with HPAM.

As depicted in Fig. 7(a), the IFT between HPAM aqueous solution and Daqing oil remains in the order of 10^1 mN·m^{-1} across all tested concentrations, while EDAB can significantly reduce the IFT to the order of 10^{-2} mN·m^{-1}. Such a difference is attributed to the non-amphiphilic of HPAM, which prevents it from adsorbing at the oil/water interface. In contrast, EDAB, as a typical zwitterionic surfactant, can effectively adsorb at the oil/water interface, leading to a substantial reduction in IFT (Zhao et al., 2012). For instance, when the concentration of EDAB is 1000 mg·L^{-1}, the oil/water IFT drops to 8×10^{-2} mN·m^{-1}, whereas the IFT in the equivalent concentration of HPAM solution remains at 1.5×10^1 mN·m^{-1}. While most surfactants employed in the Daqing oilfield are known to achieve ultra-low IFT ($< 10^{-3}$ mN·m^{-1}) (Chen et al., 2018; Sun et al., 2018; Liu et al., 2024), EDAB may not match their interfacial activity. However, EDAB offers a distinct advantage: its unique thermal viscosity-enhancing capability, which these conventional surfactants lack.

As surfactant and polymer are often mixed practically in binary chemical flooding, the interfacial activity of the mixture of EDAB and HPAM at different concentrations was also examined. The IFT of the mixed solution decreases initially with increasing EDAB fraction (f_{EDAB}), then increases again (Fig. 7(b)). When the total concentration of the mixed HPAM and EDAB solution is fixed at 2000 mg·L^{-1}, with EDAB at 500 mg·L^{-1} (25% of the total concentration), the IFT sharply decreases to 2.5×10^{-2} mN·m^{-1}. As the concentration of EDAB increases to 2000 mg·L^{-1} (100% of the total concentration), the IFT remains in the order of 10^{-2} mN·m^{-1}. This behavior arises because, in the mixed solution of EDAB and HPAM, the negatively charged polymer segments attract the positively charged EDAB molecules. This leads to localized clustering of surfactant molecules around the polymer chains at the oil/water interface (Chen et al., 2021). Additionally, the polymer's long-chain structure influences surfactant distribution, further promoting tighter molecular packing at the interface through steric hindrance

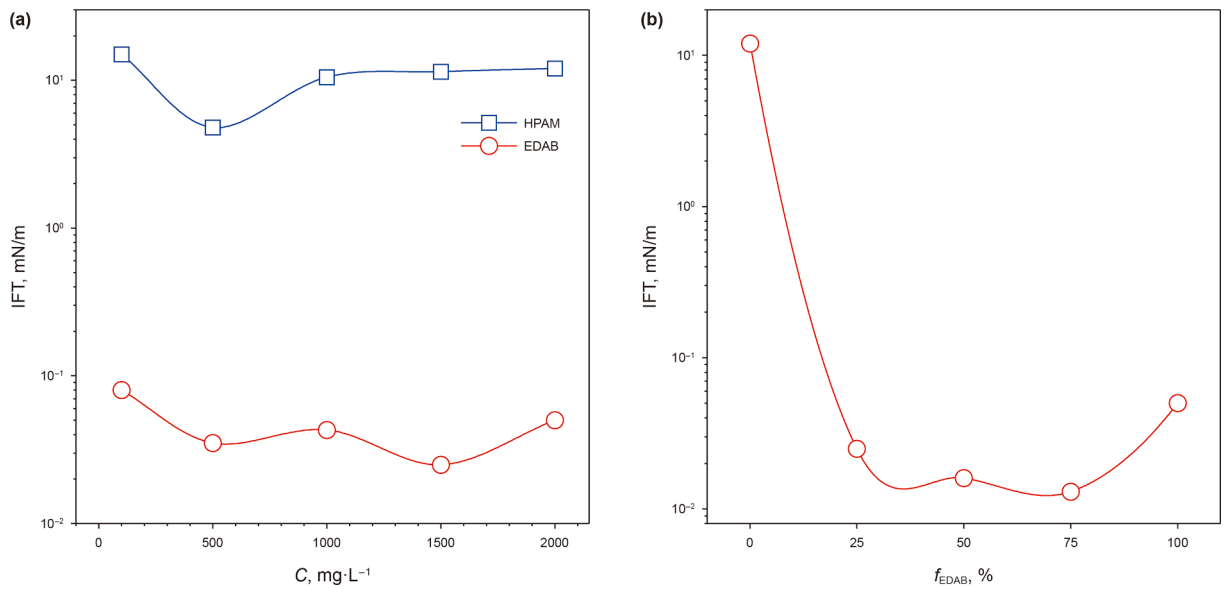

Fig. 7. IFT plotted as a function of EDAB or HPAM concentration at 45 °C. (**a**) Variation of IFT with concentration of EDAB and HPAM; (**b**) the effect of EDAB mass fraction (f_{EDAB}) on IFT of mixture of HPAM and EDAB at the fixed total concentration of 2000 mg·L^{-1}. The TDS is 4500 mg·L^{-1}.

effects (Meng et al., 2024). As a result, the IFT in the EDAB/HPAM mixed system is lower than in solutions containing EDAB alone.

3.4. Long-term thermal stability

During the displacement processes, the displacing fluid normally experiences more than six months of the transportation at the reservoir temperature. Therefore, the long-term thermal stability represents one of the most important criteria for screening chemicals for EOR use. Therefore, the long-term stability of HPAM and EDAB under simulated reservoir temperature and salinity was monitored for their effectiveness in enhancing oil recovery.

Fig. 8 shows the decay of viscosity, as well as viscosity retention of both HPAM and EDAB solutions at 45 °C and different time intervals. One can find that at the first 30 d, the viscosity of the HPAM solution significantly decreased from 36 to 18 mPa·s, with a viscosity retention of 50%. Then, at another 30-d period, the viscosity remained relatively constant. In contrast, the viscosity of the EDAB solution remained completely unchanged throughout the 60 d of aging period, holding the initial viscosity of 41 mPa·s, with a viscosity retention of 100%. This indicates that, compared to the conventional HPAM, the surfactant EDAB exhibits exceptional long-term thermal stability. During the aging process, the molecular chains of HPAM undergo thermal degradation in the saline solution, leading to a reduction in molecular weight and, consequently, a substantial decrease in solution viscosity (Doe et al., 1987). Conversely, the WLMs formed by EDAB do not experience thermal hydrolysis, which allows the viscosity of the solution to remain unchanged.

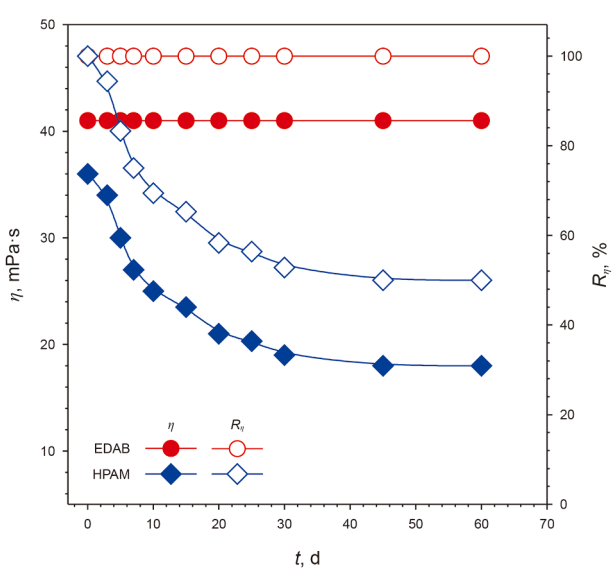

Fig. 8. Apparent viscosity (η) and viscosity retention (R_η) plotted as a function of aging time (t) for 2000 mg·L^{-1} EDAB and HPAM solutions. $\dot{\gamma}$, 10 s^{-1}; TDS, 4500 mg·L^{-1}; T, 45 °C.

In summary, the comparison results between HPAM and EDAB suggest that HPAM exhibits slightly better thickening ability; however, EDAB significantly outperforms HPAM in terms of salt tolerance, IFT reduction, and long-term stability. However, the performance difference between the two in the actual oil displacement process still needs to be investigated. Therefore, the following core flooding experiments will be carried out at simulated oil reservoir condition of Daqing Oilfield (45 °C, 4500 mg·L^{-1} NaCl). These experiments will compare the injectivity and oil recovery factor at both equal concentration (2000 mg·L^{-1}) and equal apparent viscosity (24 mPa·s) for HPAM and EDAB, as well as mixed solution of both (C_{HPAM}: $C_{EDAB} = 1:1$, $\eta = 23$ mPa·s) at total concentration of 2000 mg·L^{-1}.

3.5. Core flooding

The injectability of the displacing fluid is crucial in determining its success in EOR process (Seright et al., 2009). Therefore, the propagation of HPAM and EDAB solutions in the cores were firstly evaluated. Fig. 9 shows the flow curves of 2000 mg·L^{-1} HPAM and EDAB solutions in the cores. It can be observed that both flow curves exhibit three distinct platforms, corresponding to the stable pressure during water flooding, HPAM or EDAB flooding, and subsequent water flooding. As the polymer or surfactant solution is injected, some pore spaces in the core are blocked by polymer

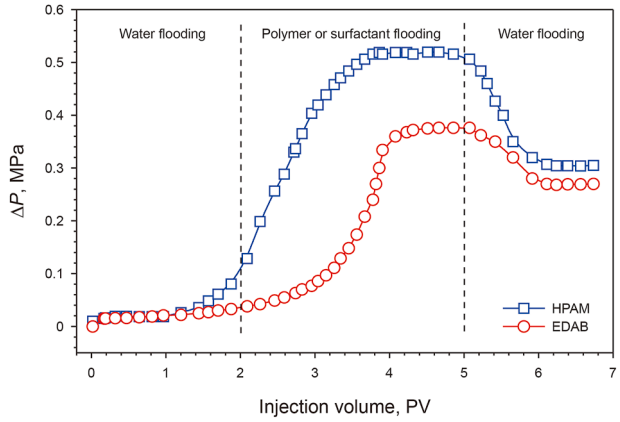

Fig. 9. Variation of flooding pressure (ΔP) during the injection of 2000 mg·L^{-1} EDAB and HPAM solutions at 0.2 mL·min^{-1} and 45 °C.

molecules or surfactant-formed micelles, causing the pressure to rise. As the injection volume increases, the injection pressure reaches its maximum and stabilizes, indicating that the polymer or surfactant solution can flow steadily through the core without plugging.

The core parameters used as well as the resistance factor (RF) and the residual resistance factor (RRF) calculated from Eqs. (3) and (4) are summarized in Table 1. The former is used to describe the reduction in oil/water mobility ratio and core permeability before and after the injection of the displacement fluid. Generally, a higher RF value implies greater flow resistance in the porous medium, which helps to expand the swept volume. The magnitude of RRF can be used to assess the ability of the displacing fluid to enhance oil recovery. However, excessively high RRF values may indicate that the displacing fluid is prone to blocking the porous medium (Zhu et al., 2022).

It can be observed that the RF (27.8) and the RRF (16.1) of the 2000 mg·L^{-1} HPAM solution are higher than those (RF, 19; RRF, 13.5) of the EDAB solution at the same concentration. This suggests that HPAM causes more significant blocking of the pore spaces during its flow through the core, resulting in greater retention inside the pores, which is beneficial for improving sweep efficiency. However, the viscosity of the 2000 mg·L^{-1} HPAM and EDAB solutions are 37 and 41 mPa·s, respectively, contradicting to the actual RF and RRF values calculated, as the higher viscosity of EDAB would typically be expected to result in greater flow resistance. In practice, however, the surfactant solution is more prone to dilution than the polymer solution during the displacement process, leading to a reduction in actual viscosity during flow and a subsequent decrease in flow resistance.

Theoretically, the higher the viscosity of a solution, the greater the pressure difference it generates during flow through pore spaces in the core. However, despite EDAB having a higher viscosity than HPAM, it exhibits lower pressure during flow. This discrepancy could be attributed to the adsorption of EDAB molecules onto the core surface. As an amphoteric surfactant, EDAB has both positive and negative charges on its hydrophilic head, which makes its charged groups prone to interacting with the rock surface, leading to adsorption (Lv et al., 2011). This adsorption reduces the effective concentration of EDAB in the solution, which in turn lowers its viscosity. It should be emphasized that surfactant adsorption and retention in reservoir are indeed important considerations. However, as reported by Morvan et al. (2009) zwitterionic surfactants like EDAB exhibit moderate adsorption in sandstone reservoirs, which falls within acceptable ranges for EOR applications. Additionally, as shown in Fig. 5, at higher shear rates, the worm-like micelle assemblies formed by the EDAB solution are more readily disassembled, further decreasing the liquid viscosity and leading to lower RF and RRF. At the same time, the degradation and retention of HPAM led to clogging of the low-permeability core, which resulted in a further decrease in the permeability of the core (Abdelgawad, 2022), leading to higher RF and RRF.

The above core injection test demonstrated that both 2000 mg·L^{-1} HPAM and EDAB solutions can be successfully transported through the cores. Therefore, by fixing the concentration of both HPAM and EDAB at 2000 mg·L^{-1}, their ability to enhance oil recovery was compared.

In the core flooding experiments, the sweep efficiency directly affects the oil recovery factor, and the sweep efficiency is influenced by the mobility ratio (M) between the displacing and displaced phases. The mobility ratio is calculated using Eq. (8), which reflects the relative flow velocities of the displacing and displaced phases (Li et al., 2017).

$$M = \frac{K_p/\eta_p}{K_o/\eta_o} \tag{8}$$

where K_o and K_p are the core permeability of the flooding phase and the flooded phase, respectively; η_o and η_p are the apparent viscosity of the flooding phase and the flooded phase, respectively.

Generally, when $M > 1$, the displacing fluid leads to a fingering phenomenon, resulting in low oil recovery efficiency. On the other hand, when $M < 1$, the displacing fluid moves forward like a piston, displacing the oil out of the pore spaces, thereby increasing the sweep area and oil recovery factor. Therefore, in the flooding process, it is important to adjust the mobility ratio of oil to displacing fluid to be less than 1 to achieve a higher oil recovery factor. The calculated mobility ratios for EDAB and HPAM are tabulated in Table 2. It can be seen that the mobility ratios of both solutions are very similar and less than 1, indicating that both solutions exhibit good sweep efficiency.

Fig. 10(a) shows the relationship between the oil recovery factor and injection pressure as a function of injection volume of 2000 mg·L^{-1} HPAM and EDAB solutions, under simulated Daqing Oilfield conditions (45 °C, 4500 mg·L^{-1} NaCl). The corresponding parameters are listed in Table 3 for Cores 3 and 4, respectively. The entire flooding process consists of three stages: water flooding, chemical flooding, and subsequent water flooding. For HPAM,

Table 2
Mobility ratios (M) for 2000 mg·L^{-1} EDAB and HPAM solutions at 45 °C.

Displacing fluid	K, mD	K_o, mD	η, mPa·s	η_o, mPa·s	M
EDAB	3.4	6.4	41	9.8	0.13
HPAM	2.6	5.7	37	9.8	0.12

Table 1
RF and RRF of 2000 mg·L^{-1} HPAM and EDAB solutions in porous media at 45 °C.

Core No.	Displacing fluid	Core length L, cm	Core diameter d, cm	PV, mL	Porosity ϕ, %	Water permeability K_w, mD	RF	RRF
1	HPAM	7.8	2.5	10.2	26.6	30	27.8	16.1
2	EDAB	7.5	2.5	9.4	25.5	25	19.0	13.5

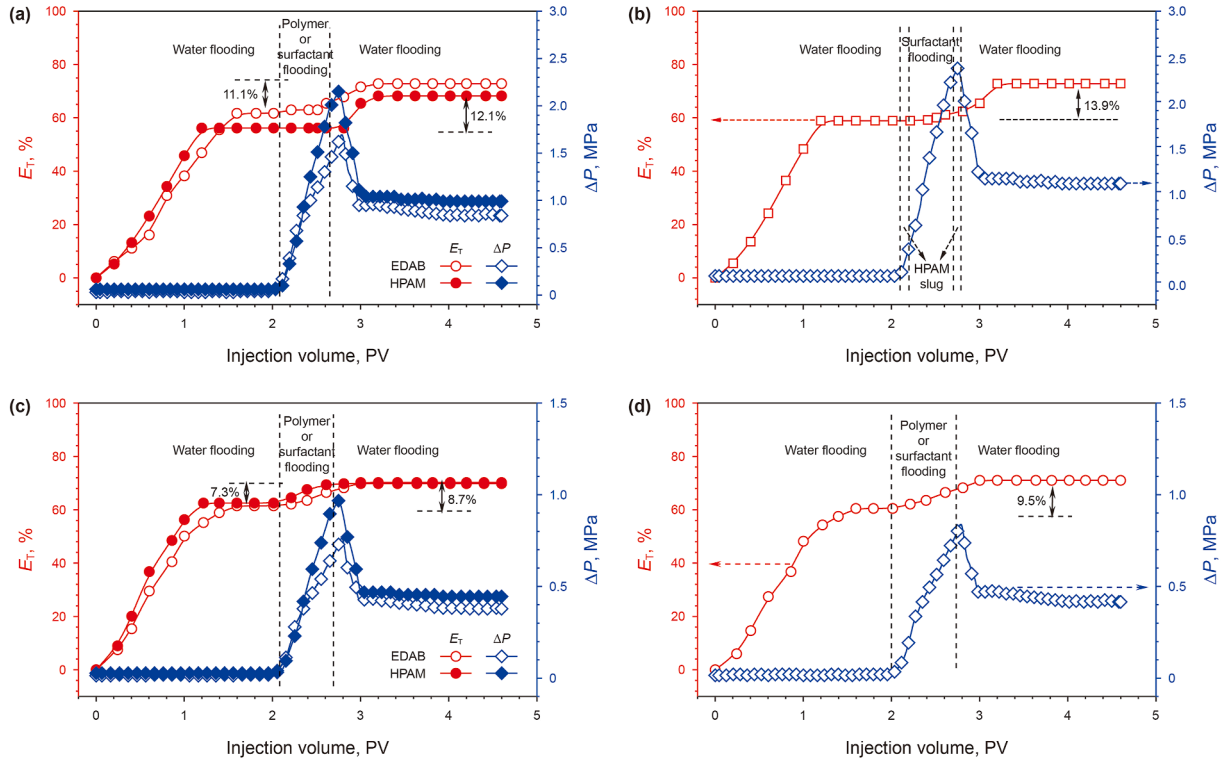

Fig. 10. Oil recovery factor and displacement pressure of the displacing fluid plotted versus injection volume. (**a**) Equal concentration (2000 mg·L^{-1}) of EDAB and HPAM solutions; (**b**) 2000 mg·L^{-1} HPAM solution as pre- and post-flooding plugs (0.1 PV respectively); (**c**) EDAB and HPAM solutions with equivalent viscosity (24 mPa·s); (**d**) mixed solution of EDAB and HPAM with total concentration of 2000 mg·L^{-1} (C_{EDAB}:C_{HPAM} = 1:1). TDS, 4500 mg·L^{-1} NaCl; T, 45 °C.

Table 3
Oil recovery factors for aqueous solutions of EDAB and HPAM in 8-cm cores.

Core No.	Displacing fluid	η, mPa·s	L, cm	d, cm	PV, cm^3	ϕ, %	K_w, mD	E_w, %	$E_{p(s)}$, %	E_T, %
3	EDAB	28	7.2	2.5	9.9	28.0	30	61.1	11.1	72.2
4	HPAM	41	6.7	2.5	9.2	27.9	31	56.2	12.1	68.3
5	EDAB	24	8.1	2.5	9.5	23.9	29	61.5	8.7	70.2
6	HPAM	24	8.1	2.5	9.5	23.9	32	62.5	7.3	69.8
7	HPAM/EDAB	41/28	8.1	2.5	8.6	21.6	28	59.0	13.9	72.9
8	HPAM-EDAB	23	8.1	2.5	8.7	21.9	30	60.5	9.5	71.0

Note: E_w is the incremental oil recovery after initial water flooding; $E_{p(s)}$ is the incremental oil recovery by HPAM or EDAB flooding; E_T is the total recovery factor.

during the water flooding stage, the recovery factor gradually increases with the injection volume until it stabilizes at 56.2%, at which point water flooding is stopped. In the chemical flooding stage, the 0.5 PV of HPAM solution injected into the core results in a gradual increase in pressure and a slight rise in recovery factor. Finally, during the subsequent water flooding stage, flooding pressure begins to decline, and the recovery factor increases, stabilizing at 68.3%. The net recovery factor by HPAM is the difference between total recovery factor and that by water flooding, that is, 12.1% of the recovery factor.

Under the same conditions, three core flooding tests were conducted with EDAB solution to verify experimental reproducibility. As shown in Figs. 10(a) and S4, the oil recovery factors of EDAB were measured as 11.1%, 11.3%, and 10.9% respectively, yielding an average recovery factor of 11.1%, which is 1% lower than that of HPAM. Table S1 lists the relevant parameters and experimental data of the core samples used in the replicate experiments. As indicated in Fig. 4, the thermal thickening ability of EDAB renders significantly higher viscosity at 45 °C compared to 25 °C, suggesting that EDAB should have a higher sweep efficiency. However, the low concentration of the EDAB solution used may result in a dilution that is not resistant to pre- and post-water flooding. This reduces the effective concentration of EDAB, diminishing the viscosity increase and lowering the sweep efficiency, which ultimately results in a lower recovery factor. Additionally, during injection, the EDAB solution mixes with the crude oil in the core, destroying the wormlike micelles formed by EDAB molecules. This further reduces the viscosity of the solution, adversely affecting the recovery factor. In other words, the thermal thickening ability of EDAB is constrained by both the rock surface and the crude oil. To minimize the impact of surfactant adsorption and mixing with oil, which leads to a reduced thermal thickening effect, we further investigated the oil recovery factor of EDAB solution when pre-HPAM and post-HPAM slug systems were applied.

As shown in Fig. 10(b), during the second stage of chemical flooding, 0.1 PV of HPAM slug was first injected into the core, followed by the EDAB solution, and then another 0.1 PV of HPAM slug. The core parameters used are shown in Core 7 of Table 3. The two slugs encapsulated the injected EDAB solution, preventing direct contact between the EDAB solution and the crude oil. This approach not only reduces the dilution of the EDAB solution by subsequent water flooding to some extent, but more importantly,

preserves the thermal thickening effect of EDAB. The water flooding stage yielded a recovery factor of 59.0%, with EDAB contributing an additional 13.9%, bringing the total to 72.9%. Compared to EDAB injection without protective slugs, the slug-assisted method improved recovery by 2.7% and outperformed HPAM. This enhancement likely stems from reduced fluid dilution (due to the HPAM slugs) and higher viscosity of EDAB, which improves sweep efficiency and ultimately boosts recovery.

Additionally, we further investigated the difference in oil recovery efficiency between EDAB and HPAM solutions at same viscosity (Fig. 10(c)), with the corresponding parameters listed in Table 3 for Cores 5, and 6, respectively. As observed, the recovery factor from HPAM and EDAB are 7.3% and 8.7%, respectively, with EDAB showing a 1.5% higher than that by HPAM. This is because, at the same viscosity, the EDAB solution exhibits higher interfacial activity than the HPAM solution, significantly reducing the IFT (as shown in Fig. 7(a)). This reduction in IFT greatly diminishes the capillary effect in the formation, improving the displacement efficiency and resulting in a higher recovery factor.

Furthermore, we examined the oil recovery factor by the mixture solution of EDAB and HPAM as a SP binary flooding system (Fig. 10(d)). The core parameters (Core 8) used are shown in Table 3. The total concentration of the system was fixed at 2000 mg·L^{-1}, with an EDAB to HPAM mass ratio of 1:1. The IFT of the SP binary system was reduced to the order of 10^{-2} mN·m^{-1} (Fig. 7), and the viscosity was approximately 23 mPa·s. Notably, the HPAM-EDAB mixture exhibits lower thickening capability compared to single-component solutions at equivalent concentrations. This behavior likely stems from competitive solvation effects: EDAB's zwitterionic headgroups form strong interactions with water molecules, potentially limiting HPAM's access to hydration layers. Consequently, the reduced solvation of HPAM chains increases their rigidity, ultimately diminishing the solution viscosity. However, the recovery factor achieved by the SP binary system was 9.5%, which is higher than that of single EDAB and HPAM slug. This improvement can be attributed to the synergistic effect in the binary system: the surfactant EDAB reduces the oil–water IFT, while HPAM ensures the viscosity of the flooding fluid. As a result, the binary system exhibits both a large sweep efficiency and low IFT, leading to enhanced oil recovery.

However, it should be noted that during the initial water injection phase, all experimental groups exhibited smooth and consistent pressure curves with minimal fluctuation (Fig. 10). Through rigorous re-examination, we conclude that the characteristically flat and stable pressure profiles observed during initial waterflooding can be primarily ascribed to two interconnected factors: the rapid breakthrough dynamics and diminished pressure differentials inherent to the 8-cm short core samples employed in this study, and the inadequate resolution (0.04 MPa) of the pressure transducers, which falls below the threshold required for capturing such subtle transient variations.

Consequently, we subsequently implemented a comparative analysis of the oil displacement efficiencies of EDAB and HPAM solutions at the equal concentration (2000 mg·L^{-1}) using standardized 30-cm Berea cores, monitored with pressure transducers of significantly enhanced precision (0.01 MPa resolution). The comprehensive petrophysical properties of the Berea cores and the corresponding core flooding experimental results are recorded in Table 4. The experimental results demonstrate that during core flooding tests using EDAB solution on long core samples, the breakthrough pressure and stabilized pressure recorded in the initial water flooding stage were 0.25 and 0.22 MPa, respectively (as shown in Fig. 11). Corresponding measurements for HPAM solution flooding yielded breakthrough and stabilized pressures of 0.30 and 0.24 MPa. This indicates minimal differentials between breakthrough and stabilized pressures ($\Delta P \leq 0.06$ MPa) during water flooding in Berea cores. Consequently, when employing short core samples where transient pressure dynamics occur within sub-detection timescales, the virtual absence of measurable differences between breakthrough and stabilized pressures becomes scientifically plausible.

For the EDAB system in long-core water flooding, the oil recovery factor progressively increased with the injection volume of brine until stabilizing at 49.4%. During the chemical flooding phase, following the injection of 0.5 PV of EDAB solution, the displacement pressure demonstrated a systematic buildup. Subsequent post-water injection triggered a gradual pressure decline while progressively enhancing oil recovery, ultimately stabilizing at 60.0%. Consequently, EDAB delivered a quantifiable

Table 4
Summary of oil recovery factors for validation experiments using Berea cores.

Core No.	Displacing fluid	η_1, mPa·s	η_2, mPa·s	L, cm	l, cm	PV, cm^3	ϕ, %	K_w, mD	E_w, %	$E_{p(s)}$, %	E_T, %
11	EDAB	28	37	30.0	4.5	86.5	20.7	53	49.4	10.6	60.0
12	HPAM	41	33	30.0	4.5	87.0	21.1	49	52.9	9.2	62.1

Note: η_1 and η_2 are the viscosity of displacing fluids (2000 mg·L^{-1}) at 25 °C and 45 °C, respectively; l is the edge length of the rectangular prismatic core sample.

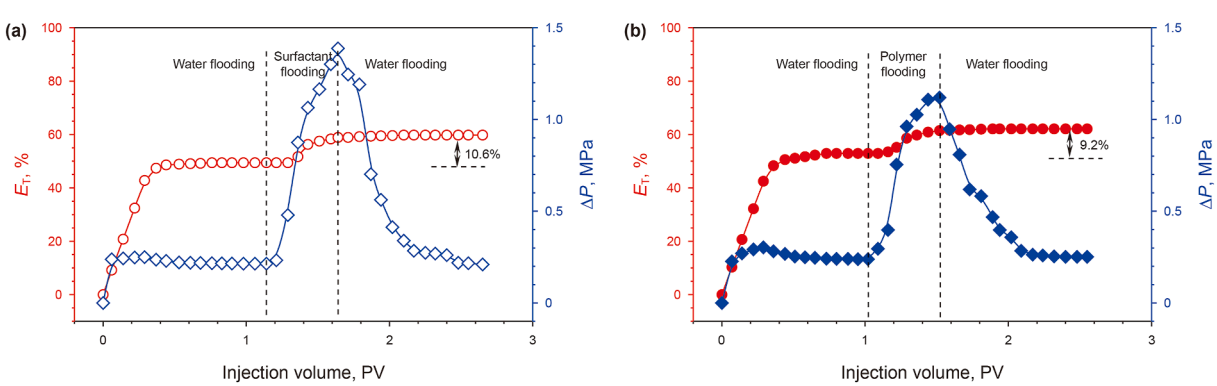

Fig. 11. Oil recovery factor and displacement pressure of the displacing fluid plotted versus injection volume. (**a**) 2000 mg·L^{-1} EDAB solution; (**b**) 2000 mg·L^{-1} HPAM solution. TDS, 4500 mg·L^{-1} NaCl; T, 45 °C.

enhancement of 10.6% in ultimate recovery (Fig. 11(a)). For the HPAM solution, both the pressure profile and oil recovery curve exhibited trends analogous to those observed with EDAB. The initial water flooding recovery factor stabilized at 52.9%, while the polymer flooding yielded an incremental recovery of 9.2% (Fig. 11(b)). As further delineated in Table 4, HPAM demonstrates higher initial injection viscosity than EDAB. Significantly, at the experimental temperature of 45 °C, EDAB exhibits superior viscosity retention alongside a 1.4% advantage in enhanced oil recovery over HPAM. This integrated performance profile mechanistically validates enhanced displacement efficacy of EDAB.

4. Conclusions

In summary, this study identifies EDAB as a promising viscoelastic surfactant alternative to conventional HPAM for EOR application in Daqing Oilfield. Our systematic evaluation demonstrates superior thermal stability, robust salt tolerance, and improved interfacial activity of EDAB. Notably, EDAB shows distinct thermo-thickening behavior—its viscosity increases by 89% over the temperature range of 25–55 °C, which aligns precisely with the temperature variation experienced by displacement fluids during injection (surface to bottomhole) and transport in porous media. Unlike HPAM, which typically suffers viscosity loss under such conditions, the viscosity of EDAB increases with temperature, offering a highly desirable performance for displacement fluids.

Additionally, EDAB demonstrates exceptional salt tolerance, retaining nearly 100% of its viscosity even at Ca^{2+} and Mg^{2+} concentrations of 80 mg/L, far surpassing HPAM's 63.5% retention. It also achieves significant IFT reduction, reaching 10^{-2} mN·m^{-1} at just 2000 mg·L^{-1}. Core-flooding tests further confirm its EOR potential, with a 10.6% incremental recovery (compared to HPAM's 9.2%) due to improved sweep efficiency and oil/water interfacial activity.

These findings position EDAB as a viable solution for EOR in saline environments where conventional EOR polymers underperform. Moving forward, research efforts should prioritize optimizing EDAB for field-scale applications, with particular attention to its interactions under varying reservoir conditions to maximize recovery efficiency and minimize adsorption losses. Additionally, enhancing EDAB's temperature and salt resistance will be crucial for extending its applicability to high-temperature, high-salinity reservoirs. Finally, developing a cost-effective and scalable synthesis method will be essential to facilitate EDAB's practical adoption in real-world settings.

CRediT authorship contribution statement

Mo-Yi Li: Writing – original draft, Methodology, Investigation, Data curation. **Quan Yin:** Methodology, Investigation, Data curation. **Bo Li:** Validation, Resources. **Rui-Bo Cao:** Validation, Resources. **Yan Zhang:** Methodology, Formal analysis. **Xue-Zhi Zhao:** Writing – review & editing, Supervision, Project administration, Methodology. **Yu-Jun Feng:** Writing – review & editing, Supervision, Project administration, Funding acquisition, Conceptualization.

Declaration of competing interest

The authors declare that they have no known competing financial interests or personal relationships that could have appeared to influence the work reported in this paper.

Acknowledgements

This work was supported by the Key Joint Fund of National Natural Science Foundation of China (U23B2085) and China National Petroleum Corporation Innovation Fund (2022DQ02-0205).

Appendix A. Supplementary data

Supplementary data to this article can be found online at https://doi.org/10.1016/j.petsci.2025.08.007.

References

Abdelgawad, K.Z., 2022. Polymer induced permeability reduction: The influence of polymer retention and porous medium properties. J. Petrol. Sci. Eng. 217, 110821. https://doi.org/10.1016/j.petrol.2022.110821.

Ahmed, M.E., Sultan, A.S., Al-Sofi, A., Al-Hashim, H.S., 2023. Optimization of surfactant-polymer flooding for enhanced oil recovery. J. Pet. Explor. Prod. Technol. 13, 2109–2123. https://doi.org/10.1007/s13202-023-01651-0.

Agharazi-Dormani, N., Hornof, V., Neale, G.H., 1990. Effects of divalent ions in surfactant flooding. J. Petrol. Sci. Eng. 4 (3), 189–196. https://doi.org/10.1016/0920-4105(90)90008-Q.

Akstinat, M.H., 1980. Polymes for enhanced oil recovery in reservoirs of extremely high salinities and high temperatures. In: SPE International Symposium on Oilfield and Geothermal Chemistry. https://doi.org/10.2118/8979-MS.

Al-Asadi, A., Somoza, A., Arce, A., Rodil, E., Soto, A., 2023. Nanofluid based on 1-dodecylpyridinium chloride for enhanced oil recovery. Pet. Sci. 20 (1), 600–610. https://doi.org/10.1016/j.petsci.2022.08.018.

Ameli, F., Moghbeli, M.R., Alashkar, A., 2019. On the effect of salinity and nanoparticles on polymer flooding in a heterogeneous porous media: Experimental and modeling approaches. J. Petrol. Sci. Eng. 174, 1152–1168. https://doi.org/10.1016/j.petrol.2018.12.015.

Bansal, V.K., Shah, D.O., 1978a. The effect of addition of ethoxylated sulfonate on salttolerance, optimal salinity, and impedance characteristics of petroleum sulfonate solutions. J. Colloid Interface Sci. 65 (3), 451–459. https://doi.org/10.1016/0021-9797(78)90096-6.

Bansal, V.K., Shah, D.O., 1978b. The effect of divalent cations (Ca^{2+} and Mg^{2+}) on the optimal salinity and salt tolerance of petroleum sulfonate and ethoxylated sulfonate mixtures in relation to improved oil recovery. J. Am. Oil Chem. Soc. 55 (3), 367–370. https://doi.org/10.1007/BF02669932.

Belhaj, A.F., Elraies, K.A., Mahmood, S.M., Zulkifli, N.N., Akbari, S., Hussien, O.S., 2020. The effect of surfactant concentration, salinity, temperature, and pH on surfactant adsorption for chemical enhanced oil recovery: A review. J. Pet. Explor. Prod. Technol. 10, 125–137. https://doi.org/10.1007/s13202-019-0685-y.

Chang, H., Zhang, Z., Wang, Q., Xu, Z., Guo, Z., Sun, H., Cao, X., Qiao, Q., 2006. Advances in polymer flooding and alkaline/surfactant/polymer processes as developed and applied in the People's Republic of China. J. Petrol. Technol. 58 (1), 84–89. https://doi.org/10.2118/89175-JPT.

Chauveteau, G., Sorbie, K.S., 1991. Mobility control by polymers. In: Bavière, M. (Ed.), Basic Concepts in Enhanced Oil Recovery Processes. Elsevier Applied Science Publisher, Amsterdam, pp. 43–87.

Chen, S., Han, M., AlSofi, A.M., 2021. Synergistic effects between different types of surfactants and an associating polymer on surfactant−polymer flooding under high-temperature and high-salinity conditions. Energy Fuels 35 (18), 14484–14498. https://doi.org/10.1021/acs.energyfuels.1c01034.

Chen, X., Li, Y., Liu, Z., Trivedi, J., Gao, W., Sui, M., 2023. Experimental investigation on the enhanced oil recovery efficiency of polymeric surfactant: Matching relationship with core and emulsification ability. Pet. Sci. 20 (1), 619–635. https://doi.org/10.1016/j.petsci.2022.11.002.

Chen, Z., Han, X., Kurnia, I., Yu, J., Zhang, G., Li, L., 2018. Adoption of phase behavior tests and negative salinity gradient concept to optimize Daqing oilfield alkaline-surfactant-polymer flooding. Fuel 232 (15), 71–80. https://doi.org/10.1016/j.fuel.2018.05.130.

Chu, Z., Feng, Y., 2009. A facile route towards the preparation of ultra-long-chain amidosulfobetaine surfactants. Synlett 20 (16), 2655–2658. https://doi.org/10.1055/s-0029-1217973.

Chu, Z., Feng, Y., 2010a. Amidosulfobetaine surfactant gels with shear banding transitions. Soft Matter 6 (24), 6065–6067. https://doi.org/10.1039/C0SM00874E.

Chu, Z., Feng, Y., 2010b. pH–switchable wormlike micelles. Chem. Commun. 46 (47), 9028–9030. https://doi.org/10.1039/C0CC02415E.

Chu, Z., Feng, Y., 2011. Thermo-switchable surfactant gel. Chem. Commun. 47 (25), 7191–7193. https://doi.org/10.1039/C1CC11428J.

Chu, Z., Feng, Y., Su, X., Han, Y., 2010. Wormlike micelles and solution properties of a C_{22}-tailed amidosulfobetaine surfactant. Langmuir 26 (11), 7783–7791. https://doi.org/10.1021/la904582w.

Croce, V., Cosgrove, T., Dreiss, C.A., King, S., Maitland, G., Hughes, T., 2005. Giant micellar worms under shear: A rheological study using SANS. Langmuir 21 (15), 6762–6768. https://doi.org/10.1021/la0479410.

Dreiss, C.A., 2007. Wormlike micelles: Where do we stand? Recent developments, linear rheology and scattering techniques. Soft Matter 3 (8), 956–970. https://doi.org/10.1039/B705775J.
Doe, P.H., Moradi-Araghi, A., Shaw, J.E., Stahl, G.A., 1987. Development and evaluation of EOR polymers suitable for hostile environments—Part 1: copolymers of vinylpyrrolidone and acrylamide. SPE Reserv. Eng. 2 (4), 461–467. https://doi.org/10.2118/14233-PA.
Gao, C., 2013. Viscosity of partially hydrolyzed polyacrylamide under shearing and heat. J. Pet. Explor. Prod. Technol. 3, 203–206. https://doi.org/10.1007/s13202-013-0051-4.
Han, T., Guo, J., Zhao, Q., Shen, T., Zhang, S., 2022. Insights into the multiple applications of modified polyacrylamide as oilfield corrosion inhibitor and water phase tackifier. Pet. Sci. 19 (1), 397–408. https://doi.org/10.1016/j.petsci.2022.01.003.
Han, Y., Feng, Y., Sun, H., Li, Zh, Han, Y., Wang, H., 2011. Wormlike micelles formed by sodium erucate in the presence of a tetraalkylammonium hydrotrope. J. Phys. Chem. B 115 (21), 6893–6902. https://doi.org/10.1021/jp2004634.
Huang, Z., Mao, J., Cun, M., Yang, X., Lin, C., Zhang, Y., Zhang, H., Mao, J., Wang, Q., Zhang, Q., Chen, A., Zhang, W., Zhou, H., He, Y., Liu, B., Xiao, Y., 2022. Polyhydroxy cationic viscoelastic surfactant for clean fracturing fluids: Study on the salt tolerance and the effect of salt on the high temperature stability of wormlike micelles. J. Mol. Liq. 366 (15), 120354. https://doi.org/10.1016/j.molliq.2022.120354.
Iyer, D., Syed, V.M.S., Srivastava, S., 2021. Influence of divalent ions on composition and viscoelasticity of polyelectrolyte complexes. J. Polym. Sci. 59 (22), 2895–2904. https://doi.org/10.1002/pol.20210668.
Jafarbeigi, E., Salimi, F., Kamari, E., Mansouri, M., 2022. Effects of modified graphene oxide (GO) nanofluid on wettability and IFT changes: Experimental study for EOR applications. Pet. Sci. 19 (4), 1779–1792. https://doi.org/10.1016/j.petsci.2021.12.022.
Jain, S., Pachisia, H., Sharma, A., Patel, S., Patel, S., Ragunathan, B., 2022. A systematic review—Chemical EOR using surfactants and polymers. Mater. Today Proc. 62 (13), 7220–7223. https://doi.org/10.1016/j.matpr.2022.03.602.
Kumar, A., Neale, G.H., Hornof, V., 1984. Effects of connate water composition on interfacial tension behavior of surfactant solutions. J. Can. Petrol. Technol. 23 (1), 37–41. https://doi.org/10.2118/84-01-03.
Kumar, R., Kalur, G.C., Ziserman, L., Danino, D., Raghavan, S.R., 2007. Wormlike micelles of a C_{22}-tailed zwitterionic betaine surfactant: From viscoelastic solutions to elastic gels. Langmuir 23 (26), 12849–12856. https://doi.org/10.1021/la7028559.
Lake, L.W., Schmidt, R.L., Venuto, P.B., 1992. A niche for enhanced oil recovery in the 1990s. Oilfield Rev. 4 (1), 55–61.
Lakatos, I., Toth, J., Bodi, T., Lakatos-Szabo, J., Berger, P.D., Lee, C., 2007. Application of viscoelastic surfactants as mobility-control agents. In: SPE International Symposium on Oilfield Chemistry. https://doi.org/10.2118/106005-MS.
Lai, N., Zhang, Y., Xu, Q., Zhou, N., Wang, H., Ye, Z.A., 2016. A water-soluble hyperbranched copolymer based on a dendritic structure for low-to-moderate permeability reservoirs. RSC Adv. 6 (39), 32586–32597. https://doi.org/10.1039/C6RA06397G.
Li, B., 2015. Synthesis and performance evaluation on a new type of salt resistant polymer. J. Yangtze Univ. (Nat. Sci. Ed.). 12 (16), 8–10. https://doi.org/10.16772/j.cnki.1673-1409.2015.16.007 (in Chinese).
Li, D., Fei, C., Wang, L., Xia, H., 2020. Research on working viscosity and influencing factors of polymer solution in seepage process. IOP Conf. Ser. Earth Environ. Sci. 514, 022047. https://doi.org/10.1088/1755-1315/514/2/022047.
Li, X., Xu, Z., Yin, H., Feng, Y., Quan, H., 2017. Comparative studies on enhanced oil recovery: Thermoviscosifying polymer versus polyacrylamide. Energy Fuels 31 (3), 2479–2487. https://doi.org/10.1021/acs.energyfuels.6b02653.
Liu, X., Wu, H., Chen, S., He, J., Yang, Z., Cheng, J., Wu, J., 2024. Study on the alkali-free three-component flooding system in the Daqing Oilfield. ACS Omega 9 (14), 16006–16015. https://doi.org/10.1021/acsomega.3c09527.
Lv, W., Bazin, B., Ma, D., Liu, Q., Han, D., Wu, K., 2011. Static and dynamic adsorption of anionic and amphoteric surfactants with and without the presence of alkali. J. Petrol. Sci. Eng. 77 (2), 209–218. https://doi.org/10.1016/j.petrol.2011.03.006.
Manichand, R.N., Seright, R., 2014. Field vs. laboratory polymer-retention values for a polymer flood in the Tambaredjo field. SPE Reservoir Eval. Eng. 17, 314–325. https://doi.org/10.2118/169027-PA.
Masuda, Y., Tang, K.C., Miyazawa, M., Tanaka, S., 1992. 1D simulation of polymer flooding including the viscoelastic effect of polymer solution. SPE Reserv. Eng. 7 (2), 247–252. https://doi.org/10.2118/19499-PA.
Meng, J., Wang, J., Wang, L., Lyu, C., Lyu, Y., Nie, B., 2024. Effects of polymer-surfactant interactions on drag reduction performance and mechanisms: Molecular dynamics simulations and experimentation. Colloids Surf., A 684 (5), 133126. https://doi.org/10.1016/j.colsurfa.2023.133126.
Morvan, M., Degré, G., Leng, J., Masselon, C., Moreau, P., Bouillot, J., Zaitoun, A., 2009. New viscoelastic fluid for chemical EOR. In: SPE International Symposium on Oilfield Chemistry. https://doi.org/10.2118/121675-MS.
Muller, G., 1981a. Thermal stability of high-molecular-weight polyacrylamide aqueous solutions. Polym. Bull. 5 (1), 31–37. https://doi.org/10.1007/BF00255084.
Muller, G., 1981b. Thermal stability of polyacrylamide solutions: Effect of residual impurities in the molecular-weight-degradation process upon heating. Polym. Bull. 5 (1), 39–45. https://doi.org/10.1007/BF00255085.
Pu, W., Jiang, F., He, Y., Wei, B., Tang, Y., 2016. Synthesis of a novel comb micro-block hydrophobically associating copolymer for Ca^{2+}/Mg^{2+} resistance. RSC Adv. 6 (49), 43634–43637. https://doi.org/10.1039/C6RA07110D.
Raffa, P., Broekhuis, A.A., Picchioni, F., 2016. Polymeric surfactants for enhanced oil recovery: A review. J. Petrol. Sci. Eng. 145, 723–733. https://doi.org/10.1016/j.petrol.2016.07.007.
Raghavan, S.R., Kaler, E.W., 2001. Highly viscoelastic wormlike micellar solutions formed by cationic surfactants with long unsaturated tails. Langmuir 17 (2), 300–306. https://doi.org/10.1021/la0007933.
Rai, K., Johns, R.T., Lake, L.W., Delshad, M., 2009. Oil-recovery predictions for surfactant polymer flooding. In: SPE Annual Technical Conference and Exhibition. https://doi.org/10.2118/124001-MS.
Sandrea, I., Sandrea, R., 2007. Global oil reserves–1: Recovery factors leave vast target for EOR technologies. Oil Gas J. 105 (41), 44–48.
Seright, R.S., 1983. The effects of mechanical degradation and viscoelastic behavior on injectivity of polyacrylamide solutions. SPE J. 23 (3), 475–485. https://doi.org/10.2118/9297-PA.
Seright, R.S., Seheult, M., Talashek, T., 2009. Injectivity characteristics of EOR polymers. SPE Res. Eval. Eng. 12 (5), 783–792. https://doi.org/10.2118/115142-PA.
Seright, R.S., Wang, D., 2023. Polymer flooding: Current status and future directions. Pet. Sci. 20 (2), 910–921. https://doi.org/10.1016/j.petsci.2023.02.002.
Sun, C., Guo, H., Li, Y., Song, K., 2020. Recent advances of surfactant-polymer (SP) flooding enhanced oil recovery field tests in China. Geofluids 2020 (1), 8286706. https://doi.org/10.1155/2020/8286706.
Sun, L., Wu, X., Zhou, W., Li, X., Han, P., 2018. Technologies of enhancing oil recovery by chemical flooding in Daqing Oilfield, NE China. Petrol. Explor. Dev. 45 (4), 673–684. https://doi.org/10.1016/S1876-3804(18)30071-5.
Thomas, S., 2008. Enhanced oil recovery–An overview. Oil Gas Sci. Technol. 63 (1), 9–19. https://doi.org/10.2516/ogst:2007060.
Wang, D., Cheng, J., Yang, Q., Gong, W., Li, Q., 2000. Viscous-elastic polymer can increase microscale displacement efficiency in cores. In: SPE Annual Technical Conference and Exhibition. https://doi.org/10.2118/63227-MS.
Xu, T., Mao, J., Zhang, Y., Yang, X., Lin, C., Du, A., Zhang, H., 2021. Application of gemini viscoelastic surfactant with high salt in brine-based fracturing fluid. Colloids Surf., A 611 (20), 125838. https://doi.org/10.1016/j.colsurfa.2020.125838.
Xue, X., Zhu, S., Ma, X., Zhang, S., Yang, S., Huang, Z., Xu, M., Huang, H., 2024. Enhancing heavy-oil displacement efficiency through viscoelasticity of polymer solution by investigating the viscosity limit of crude oil: An experimental study. Energy Sci. Eng. 12 (6), 2493–2504. https://doi.org/10.1002/ese3.1753.
Yang, J., 2002. Viscoelastic wormlike micelles and their applications. Curr. Opin. Colloid Interface Sci. 7 (5–6), 276–281. https://doi.org/10.1016/S1359-0294(02)00071-7.
Yang, M.H., 2001. The rheological behavior of polyacrylamide solution II. Yield stress. Polym. Test. 20, 635–642. https://doi.org/10.1016/S0142-9418(00)00084-2.
Yin, Q., Tian, Q., Doutch, J., Frimpong, A.O., Xu, X., Yin, H., Li, P., Feng, Y., 2022. An insight into the thermo-thickening behavior of wormlike micellar solutions based on ultra-long-chain surfactants. Phys. Chem. Chem. Phys. 24, 11112. https://doi.org/10.1039/D2CP00687A.
Zaitoun, A., Poitie, B., 1983. Limiting conditions for the use of hydrolyzed polyacrylamides in brines containing divalent ions. In: SPE International Symposium on Oilfield and Geothermal Chemistry. https://doi.org/10.2118/11785-MS.
Zamani, A.M., Moslemi, A., Hassani, K., 2024. Experimental investigation into effects of the natural polymer and nanoclay particles on the EOR performance of chemical flooding in carbonate reservoirs. Pet. Sci. 21 (2), 951–961. https://doi.org/10.1016/j.petsci.2023.11.001.
Zeynalli, M., Mushtaq, M., Al-Shalabi, E.W., Alfazazi, U., Hassan, A.M., AlAmeri, W., 2023. A comprehensive review of viscoelastic polymer flooding in sandstone and carbonate rocks. Sci. Rep. 13 (1), 17679. https://doi.org/10.1038/s41598-023-44896-9.
Zhang, Y., Zhou, D., Ran, H., Dai, H., An, P., He, S., 2015. Rheology behaviors of C_{22}-tailed carboxylbetaine in high-salinity solution. J. Dispersion Sci. Technol. 37 (4), 496–503. https://doi.org/10.1080/01932691.2015.1045601.
Zhao, R.H., Huang, H.Y., Wang, H.Y., Zhang, J.C., Zhang, L., Zhang, L., Zhao, S., 2012. Effect of organic additives and crude oil fractions on interfacial tensions of alkyl benzene sulfonates. J. Dispersion Sci. Technol. 34 (5), 148–156. https://doi.org/10.1080/01932691.2012.685844.
Zhong, H., He, Y., Yang, E., Bi, Y., Yang, T., 2022. Modeling of microflow during viscoelastic polymer flooding in heterogenous reservoirs of Daqing Oilfield. J. Petrol. Sci. Eng. 210, 110091. https://doi.org/10.1016/j.petrol.2021.110091.
Zhu, S., Zhang, S., Xue, X., Zhang, J., Xu, J., Liu, Z., 2022. Influencing factors for effective establishment of residual resistance factor of polymer solution in porous media. J. Polym. Res. 29, 210. https://doi.org/10.1007/s10965-022-03066-7.
Zilz, J., Schäfer, C., Wagner, C., Poole, R.J., Alves, M.A., Lindner, A., 2014. Serpentine channels: Micro-rheometers for fluid relaxation times. Lab Chip 14 (2), 351–358. https://doi.org/10.1039/C3LC50809A.